



Discrimination of Phosgene from Cyanogen Chloride in Recovered Chemical Munitions Using Tagged Neutron Interrogation with High-Resolution Gamma-Ray Spectroscopy

Changing the World's Energy Future

Brian M Bucher, Edward H Seabury, Jay D Hix, Kenneth M Krebs, Jayson Wharton, Paul Hausladen, Seth McConchie



DISCLAIMER

This information was prepared as an account of work sponsored by an agency of the U.S. Government. Neither the U.S. Government nor any agency thereof, nor any of their employees, makes any warranty, expressed or implied, or assumes any legal liability or responsibility for the accuracy, completeness, or usefulness, of any information, apparatus, product, or process disclosed, or represents that its use would not infringe privately owned rights. References herein to any specific commercial product, process, or service by trade name, trade mark, manufacturer, or otherwise, does not necessarily constitute or imply its endorsement, recommendation, or favoring by the U.S. Government or any agency thereof. The views and opinions of authors expressed herein do not necessarily state or reflect those of the U.S. Government or any agency thereof.

Discrimination of Phosgene from Cyanogen Chloride in Recovered Chemical Munitions Using Tagged Neutron Interrogation with High-Resolution Gamma- Ray Spectroscopy

**Brian M Bucher, Edward H Seabury, Jay D Hix, Kenneth M Krebs, Jayson
Wharton, Paul Hausladen, Seth McConchie**

February 2023

**Idaho National Laboratory
Idaho Falls, Idaho 83415**

<http://www.inl.gov>

**Prepared for the
U.S. Department of Energy
Under DOE Idaho Operations Office
Contract DE-AC07-05ID14517, DE-AC07-05ID14517**

Discrimination of Phosgene from Cyanogen Chloride in Recovered Chemical Munitions Using Tagged Neutron Interrogation with High-Resolution Gamma-Ray Spectroscopy

B. Bucher*, E.H. Seabury, J. Hix, K.M. Krebs, C.J. Wharton

Nuclear Nonproliferation Division, Idaho National Laboratory, Idaho Falls, ID 83415, USA

S.M. McConchie, P.A. Hausladen

Physics Division, Oak Ridge National Laboratory, Oak Ridge, TN 37831, USA

Abstract

The associated particle (AP) technique has recently been used with a high-purity germanium γ -ray spectrometer to assess its capability to improve field identification of recovered chemical warfare (CW) materiel through prompt gamma-ray neutron activation analysis (PGNAA) measurements. A particularly challenging pair of CW agents commonly found in recovered munitions are phosgene (CG) and cyanogen chloride (CK), which have two of three elements in common, i.e. chlorine and carbon, but differ in the third being either oxygen or nitrogen. The detection of both latter elements is complicated by high oxygen concentration in the field environment which interferes with the small signal produced from the chemical agents. The matter is further complicated by the precautionary field practice of overpacking recovered munitions with vermiculite in larger steel multiple round containers (MRCs), which places additional oxygen-rich material in contact with the munition while further attenuating an already weak signal emitted from the munition center. This work reports quantitative results from realistic field measurements of CG and CK simulants in mock 4.2-inch (11 cm) mortar rounds overpacked with vermiculite in a large MRC. Results obtained with the AP technique are compared to those obtained with the traditional PGNAA approach for both overpacked- and bare-munition measurements. The AP technique is shown to provide a much more confident discrimination between the two chemicals, particularly for the more challenging field-relevant overpacked measurements, where a significant gain in sensitivity to all the key elements (chlorine, carbon, nitrogen and oxygen) is achieved.

Keywords: Active Neutron Interrogation, Associated Particle Technique, Recovered Chemical Warfare Materiel, Phosgene, Cyanogen Chloride

1. Introduction

During the First World War and the ensuing decades, the United States military produced, tested, and stockpiled large quantities of chemical weapons. Prior to the increasing recognition of environmental, health, and safety concerns in the 1960s, expired and obsolete munitions were often disposed of simply by open pit burning, burial in trenches, or dumping in the sea (DENIX - DoD Environment, Safety and Occupational Health Network and Information Exchange; National Research Council, 2012). Although the vast majority of modern stockpiled chemical warfare (CW) munitions have been safely destroyed following the signing and ratification of the Chemical Weapons Convention (CWC) (Organisation for the Prohibition of Chemical Weapons) in the 1990s, with the remaining few

percent expected to finally be destroyed within the next year or so (Campbell, 2022; Fazili et al., 2022), there are still large quantities of old CW munitions that will continue to be recovered from the nearly 250 estimated burial sites in the U.S. (National Research Council, 2012; Carton et al., 2016) for the foreseeable future through various environmental remediation, range clearing, or commercial activities that may turn up such items. Although the CWC does not require the recovery of these items, once they do turn up, the treaty requires that they be declared and destroyed. In many cases, these items are uncovered in areas also containing non-CW munitions and are heavily damaged following years of exposure to the elements making it impossible to identify their contents based on any markings that may have originally been imprinted on their surfaces during production. Therefore any suspect items containing a liquid fill must be assessed to determine if CW agent is present prior to disposal.

Given the potential lethality of CW agents, safety con-

*Corresponding author

Email address: brian.bucher@inl.gov (B. Bucher*)

cerns have required the development of nondestructive analysis methods for field-recovered munitions. In particular, neutron activation analysis of prompt γ rays (PGNAA) can readily identify the fill chemicals within a munition. A typical PGNAA device is the portable isotopic neutron spectroscopy (PINS) system (U.S. Army Chemical Materials Activity, c; Idaho National Laboratory). PINS has been used for over three decades to identify a wide variety of suspect CW munitions (Caffrey et al., 1992).

A standard PINS system uses a ^{252}Cf spontaneous fission source to irradiate items with neutrons, however most of those neutrons are not energetic enough to excite carbon and oxygen which are important for identifying conventional explosives along with certain CW agents. To help overcome this lack of sensitivity, a PINS system utilizing a deuterium-tritium (DT) neutron generator has been developed which produces 14-MeV neutrons that can easily excite carbon and oxygen nuclei through inelastic scattering and, thus, induce their characteristic γ ray emission. However the highly-penetrating fast neutrons also interact in the surrounding environment where these same elements are often more abundant, causing an intense background that can overwhelm the signal produced by the test item itself. Moreover, the high background can also hide low-intensity lines such as those produced from nitrogen, which are also key to identifying explosives and various CW agents along with any other energetics that may be present in the munition components (National Research Council, 2012; Caffrey et al., 1992; Bucher et al., 2022).

One particular situation where this high background and corresponding lack of sensitivity becomes an issue is in the discrimination of cyanogen chloride (NATO code CK, chemical formula CNCl) from carbonyl dichloride (code CG, formula COCl_2 , more commonly known as phosgene). Each is listed as a Schedule 3 chemical under the CWC (Organisation for the Prohibition of Chemical Weapons); both have important industrial purposes but also were heavily produced and stockpiled as chemical weapons by the U.S. military through the years (DENIX - DoD Environment, Safety and Occupational Health Network and Information Exchange; National Research Council, 2012). Following the development of nerve agents and, not to mention, nuclear weapons in the post-World War II years, they largely became obsolete and were replaced. Consequently, both are commonly encountered in recovered chemical munitions. As discussed by Bucher et al. (2022) and elucidated in the present manuscript, these two agents look nearly identical in a traditional PGNAA measurement with a standard DT generator-based PINS system, largely due to high oxygen backgrounds.

It is important to be able to distinguish the two for a couple of reasons. First, CK can become explosively unstable over time due to polymerization (Compton, 1987), and therefore requires extra care when handling. The other main reason is related to the safe monitoring of the neutralization and destruction procedures carried out using the Explosive Destructive System (EDS) (U.S. Army

Chemical Materials Activity, a), which is the most common method utilized for recovered CW munition disposal. Although both CK and CG are typically neutralized using an aqueous NaOH reagent, the resulting reaction products will differ depending on which agent is being neutralized, and a misidentification could result in an erroneous assessment of the neutralization process potentially causing an unsafe situation. Furthermore, the neutralization of CG with NaOH has a number of drawbacks, and other possible reagents are currently being examined (Carlson and Crocker, 2021) which may result in different treatments for the two agents altogether. Thus an improved discriminability is necessary.

Recently, the associated particle (AP) technique was tested with a PINS-like high-resolution germanium-based PGNAA system to determine if any improvements in sensitivity and discriminability could be achieved with the strong background suppressibility inherent to this method (Bucher et al., 2022). A variety of simulated CW agents in thick, steel mock munition containers were tested, all yielding promising results. In particular, a comparison between CK and CG simulants revealed a critical advantage of the AP technique in its ability to completely remove background oxygen from the otherwise oxygen-free CK spectrum, enabling the detection of its weak nitrogen signal and thus allowing the two agents to be easily distinguished.

In actual field scenarios, however, the situation is a bit more challenging, because recovered munitions are typically overpacked with vermiculite in Multiple Round Containers (MRCs) for safe handling and transport and to prevent potential exposure to personnel or the environment in case of leaks (National Research Council, 2012; U.S. Army Chemical Materials Activity, b). Vermiculite is a low-density material composed mainly of various oxides of Al, Mg, Si, and Fe (Papadopoulos et al., 2008). The MRCs come in a range of sizes and are constructed of thick stainless steel and DOT-certified for transport on public roads enabling relocation to more safe and secure premises if needed. There are a number of negative effects that overpacking has on the PGNAA measurements: namely increased attenuation of characteristic γ rays produced from the chemical munition fill, a higher flux of characteristic Fe and Compton background γ rays due to neutron interactions inside the MRC, and additional neutron scatter into the germanium detector and surrounding shield materials which contribute further to the observed background signal.

The purpose of this work was to provide a quantitative examination of the effect of overpacking in a MRC on the detectability and discriminability of CK and CG simulants contained in mock 4.2-inch (11 cm) mortar shells and to assess any overall improvements achieved with the AP technique. The following sections provide a more complete analysis and set of results for the bare munition measurements first presented by Bucher et al. (2022) along with analogous, follow-up measurements of those same simu-

lants and mock munitions overpacked with vermiculite in a MRC. Results obtained utilizing the AP method (i.e. neutron tagging by α -coincidence gating) are compared with those obtained using the traditional PGNA method (no coincidence gating). Additional results related to detector timing and α pulse height analyses are also presented.

2. Experimental Setup

The measurements were conducted at the Idaho National Laboratory (INL) PINS facility which contains a large experimental vault constructed of concrete and equipped with a safety interlock system that is well-suited for PGNA experiments using fast neutrons (Chichester et al., 2009). A Thermo Scientific model API-120 DT neutron generator (Chichester et al., 2005) was arranged in the center of the vault, held horizontally 36 cm above the floor on steel jack stands. An Ortec GMX series PopTop liquid nitrogen cooled high-purity germanium (HPGe) detector of 43% relative efficiency was centered in the same horizontal plane parallel to the floor, suspended by a small, steel cart. The API-120 included a thin, YAP(Ce) scintillator coupled to a sapphire viewport used to detect the associated α particles created with each neutron generated inside the device. The scintillation pulses were converted to electronic pulses by a Hamamatsu R580 photomultiplier tube (PMT), which was coupled to the sapphire viewport with optical silicon grease. Both the HPGe and PMT outputs were fed into a XIA Pixie-4e digital pulse processor data acquisition system which provided event-by-event time stamps and pulse heights for HPGe singles and YAP-coincidences (see Bucher et al. (2022) for details).

The API-120 was operated at 85 kV acceleration potential with 50 μ A of beam current providing a neutron output of 10^7 n/s. A shadow shield consisting of a 10-cm thick block of polyethylene and 7.6 cm block of tungsten were placed between the neutron generator and HPGe to protect the latter from direct neutron bombardment. A 1.4-cm thick bismuth collimator was also placed around the HPGe to shield γ rays originating from the surrounding environment. The CW simulants and their containers were placed in front of the neutron generator and HPGe detector, forming a rough 90° angle between the two, as shown in Fig. 1 and described by Bucher et al. (2022).

Two separate configurations were studied for each of the two simulants investigated. The first configuration had the simulants contained within mock 4.2-inch (11 cm) steel mortar casings situated on an aluminum lab jack (Fig. 1 left side, see also Bucher et al. (2022)). The other configuration had the lab jack removed and the mock mortar shells overpacked with vermiculite in a large MRC (right side of Fig. 1). The elemental compositions of the two simulants used are shown in Table 1 and compared to their corresponding real CW agents. The CG simulant was 2.4 kg consisting of 80% (by mass) hexachloroethane (C_2Cl_6) and 20% silicon dioxide (SiO_2), while the CK simulant was 2.6 kg of 100% cyanuric chloride ($C_3Cl_3N_3$). Be-

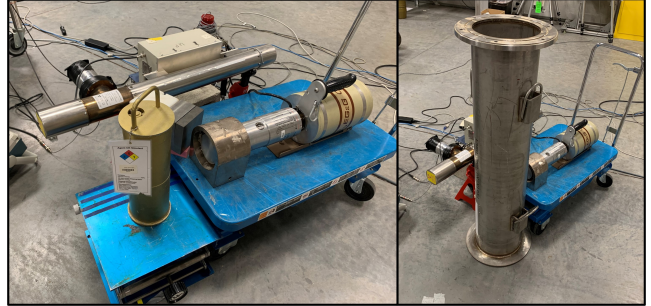


Figure 1: Experimental configurations for the bare (left) and overpacked (right) munition measurements.

Table 1: Elemental mass fractions of CK ($CNCl$) and CG ($COCl_2$) and their simulants used in the present measurements. The CK simulant was $C_3Cl_3N_3$ while the CG simulant was $C_2Cl_6+SiO_2$ (see text). Note the addition of Si in the CG simulant is not present in the real agent.

Element	CK	CK sim.	CG	CG sim.
C	19.5%	19.5%	12.1%	8.1%
N	22.8%	22.8%		
O			16.2%	10.7%
Cl	57.7%	57.7%	71.7%	71.9%
Si				9.3%

cause of multiple hazards associated with the latter, especially the high toxicity by inhalation (National Center for Biotechnology Information), that simulant was enclosed in its own unique mock mortar shell which was welded shut and had slightly different dimensions than the one used for the CG simulant as described by Bucher et al. (2022). A comparison of the two is shown in Fig. 2. The CK simulant shell was somewhat smaller having a height of 31.75 cm and inner diameter of 10.2 cm with 4.1 mm thickness, compared to that used for the CG simulant, which had a height of 35.6 cm, diameter of 11.4 cm, and thickness of 6.4 mm.

The MRC used for the overpacked measurements was larger than the ones typically used for 4.2-inch (11 cm) mortar shells found in the field. It had a height of 107 cm and inner diameter of 23 cm, which is a size more commonly used for 155-mm projectiles, whereas 4.2-inch (11 cm) mortar shells are normally overpacked in smaller MRCs having a height of 69 cm and diameter 18 cm (National Research Council, 2012; U.S. Army Chemical Materials Activity, b). This resulted in substantially more vermiculite included in the laboratory measurements compared to what would be assayed in the field. For example, the CK simulant container used in the present measurement had a 10.9 cm outer diameter which meant a 6.1-cm thick layer of vermiculite surrounded it in the overpacked MRC, whereas the analogous field measurement would normally only have a 3.6-cm thick layer of vermiculite. Therefore the measurements reported here can be considered a worst-case scenario as far as the vermiculite contribution to the spectra is concerned. Figure 3 shows one of the mock



Figure 2: Mock 4.2-inch mortar casings used to contain the CK (left most) and CG (right most) simulants. Identical empty containers (center) were also used in the overpacked measurements to examine the spectral component arising from the vermiculite and munition casing (see text for details).

munitions placed inside the MRC and overpacked with vermiculite for laboratory measurements. For each overpacked measurement, the bottom of the MRC was filled with vermiculite to a height such that the center of the container was positioned in the horizontal plane of the neutron generator and HPGe detector. Then the remaining space around and above the mock munitions was filled with vermiculite as shown in the bottom photo of Fig. 3.

Both simulants were assayed in each of the two configurations for 1 hour at a time which was equivalent to approximately 3000 live seconds, standard for most PINS measurements performed in the field. Additionally, background measurements of 20-minutes duration (~ 1000 live seconds) were recorded for both configurations, also standard for PINS field assessments. The specific live/dead times are shown in Table 2. Note the slightly higher dead times observed in the measurements of CG are due to the higher mass containers compared to those used in the measurements of CK. When assaying an overpacked munition in the field, the background is normally recorded with the entire MRC absent. The same was done in the present experiment. However, additional 20-minute background measurements were also recorded, including one with an empty MRC and one with an empty mortar shell for each simulant (Fig. 2) overpacked with vermiculite, as shown in Fig. 3. In this way, the various individual spectral contributions could be studied and compared with the results recorded with the CW simulants present. Of particular interest are the individual carbon and oxygen components measured, especially those due to the vermiculite.

3. Analysis

The Pixie-4e pulse processing unit that was used to acquire data had a 14-bit digitizing ADC with a 500-MHz

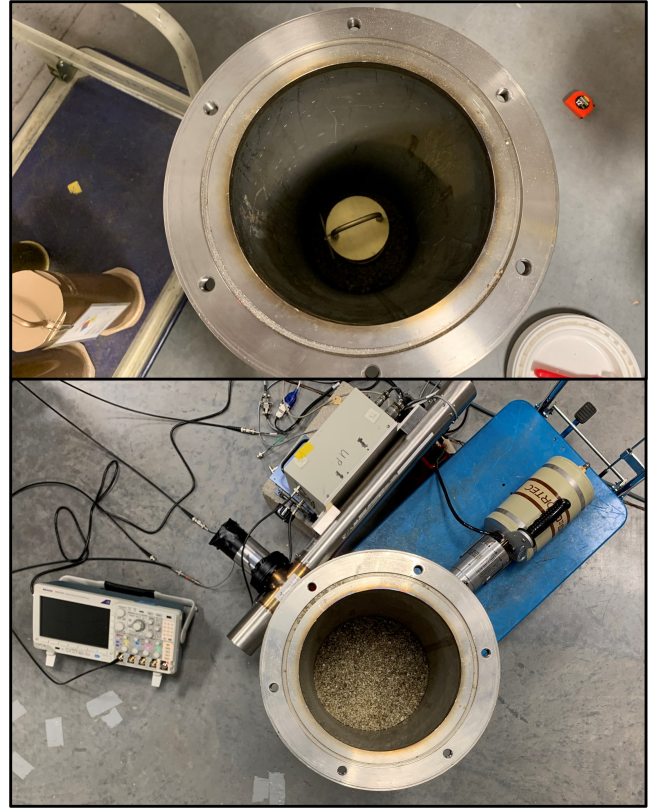


Figure 3: The mock munition is placed on top of a layer of vermiculite and centered within the MRC (upper photo) with the remaining space then filled in with more vermiculite several cm above the top of the munition (lower photo).

Table 2: Various measurements recorded with their total count times (in seconds) and corresponding live and dead times as determined by the Pixie-4e pulse processing unit.

Meas. Config.	Count Time	Live Time	Dead Time
Bare Background	1200	1067	11.1%
Bare CK	3600	3112	13.6%
Bare CG	3600	3061	15.0%
Overpacked Bkgd	1200	1074	10.5%
Empty MRC	1200	1021	14.9%
Ovpk Empty CK	1200	1001	16.6%
Overpacked CK	3600	2983	17.1%
Ovpk Empty CG	1200	995	17.1%
Overpacked CG	3600	2920	18.9%

sampling rate and was configured for list mode runs as described by Bucher et al. (2022). In this mode, the outputs from the YAP PMT and preamplifier of the HPGe detector are each fed directly into separate input channels of the digitizer. All HPGe events passing the threshold and pulse pileup inspections were recorded, which consisted of 64k channel resolution pulse heights and nanosecond-precision time stamps (XIA). YAP events, on the other hand, were only recorded if they occurred in coincidence with a HPGe event within a 600-ns window. The data were sorted offline and analyzed using the ROOT data analysis framework (Brun and Rademakers, 1997).

The inset of Fig. 4 shows the YAP-HPGe time spectrum recorded for the bare-munition CK simulant. A large, true-coincidence time peak is observed at $\Delta T=0$ sitting on top of a flat, uncorrelated background comprised of random coincidence events. HPGe spectra corresponding to various slices of the true-coincidence time spectrum are shown in the top portion of Fig. 4. In each spectrum, the random events have been subtracted out using the coincidence gate between -300 ns and -100 ns (gray box) and normalizing to match the width of each true-coincidence gate. The low-energy regions of the HPGe spectra are expanded at the bottom of Fig. 4.

It is apparent from Fig. 4 that the vast majority of prompt γ rays with energies greater than ~ 1 MeV are recorded within the first 40 ns on the rising edge of the true-coincidence time peak. Later slices along the falling edge of the time peak consist of lower and lower-energy γ rays. This is suggestive of an amplitude walk effect present in the Pixie-4e leading edge time pick-off method (XIA; Knoll, 1979); the effect becoming increasingly dramatic as pulse heights decrease towards the threshold setting. Indeed, this is confirmed by the HPGe time response curve shown in Fig. 5. The response curve was generated by gating on fine slices of the Compton continuum in the HPGe coincidence spectrum recorded from the bare-munition CK measurement, taking care to avoid any photopeaks. The time projections of each Compton slice relative to their coincident YAP α events show individual correlated time peaks (see inset of Fig. 5) whose centroids and widths vary with energy. A Gaussian function was used to fit each time peak and extract the individual centroids and widths plotted in Fig. 5. The measured time response is fairly uniform down to a few hundred keV where the amplitude walk and time resolutions began to rapidly worsen with lower energies.

Interestingly, a similar timing analysis of the individual photopeaks reveals a range of time-delays relative to the Compton continuum, typically falling between ± 5 ns, which appears to be correlated with the element response and the threshold energy required to induce that particular photopeak. This is not so surprising since one might expect γ rays arising from the fastest neutrons interacting with elements nearest the neutron generator to arrive earliest, while down-scattered neutrons interacting with materials further away should arrive later. For exam-

ple, lines arising from $(n,2n)$ reactions tend to arrive a few ns earlier than Compton events of the same γ -ray energy while many (n,n') lines arrive at the same time or later than their underlying Compton events. Bismuth γ rays, which are induced by neutrons scattered into the HPGe collimator, arrive later than their counterparts induced in the steel munition casing or chemical simulant. The time shifts of photopeaks are relatively small compared to the overall resolution and energy-dependent time walk (Fig. 5) and can generally be neglected when choosing the coincidence time gate, provided the latter is sufficiently wide.

As an example, the timing analysis of the strong Cl line at 2128 keV is shown at the bottom right of Fig. 5. The time distribution of the Compton events has been subtracted out leaving a time peak with a centroid at $-11.7(3)$ ns which is $2.5(5)$ ns earlier than the Compton itself. The 2128-keV peak arises from the $^{35}\text{Cl}(n,d_1)$ reaction and requires an incident neutron energy (E_n) of at least 6.5 MeV. For comparison the 788-keV $^{37}\text{Cl}(n,2n_1)$ line ($E_n > 11.4$ MeV) and the 1763-keV $^{35}\text{Cl}(n,n'_2)$ ($E_n > 1.8$ MeV) have relative centroid shifts of $-5.4(13)$ ns and $-0.2(7)$ ns, respectively. The 896-keV $^{209}\text{Bi}(n,n'_1)$ line ($E_n > 0.9$ MeV) had the longest delay of those examined with a relative shift of $+7.8(12)$ ns. A more detailed analysis of the timing properties of characteristic γ rays may be of interest for future investigations, but is beyond the scope of the present study.

It should also be possible to improve the timing resolution of the system through the use of a fast constant fraction discrimination algorithm on the fully digitized waveforms, available as an add-on to the Pixie-4e pulse processing firmware. This would, furthermore, reduce the large amplitude walk observed, which is an artifact of the leading edge timing method used in the system's standard pulse processing firmware. Other minor improvements might also be achieved using a faster energy filter range on the Pixie-4e, which would improve the YAP energy resolution, as discussed by Bucher et al. (2022), and allow for an energy-walk correction in that detector if needed. An improved YAP energy resolution would also benefit the α pulse height analysis presented later in this section.

As far as the analysis and comparison between the CK and CG simulants are concerned, the most important γ rays are the Cl 2128-keV line, the O 6129-keV line and its single- and double-escape peaks (SEP/DEP), the broad 4439-keV C line, and the N 5105-keV line and its SEP along with the lower-energy 728-keV N line. Ideally a single AP coincidence gate could be utilized to analyze the full range of relevant γ rays. This was attempted first using a 72-ns wide gate starting at -32 ns in the YAP-HPGe time spectrum, however it was found that such a wide gate resulted in an unnecessary loss in precision due to the larger number of random coincidences that need to be subtracted out. This was particularly evident in the overpacked measurements which had higher event rates due to the much larger mass of material in front of the detector, with weak peaks like those from nitrogen typically

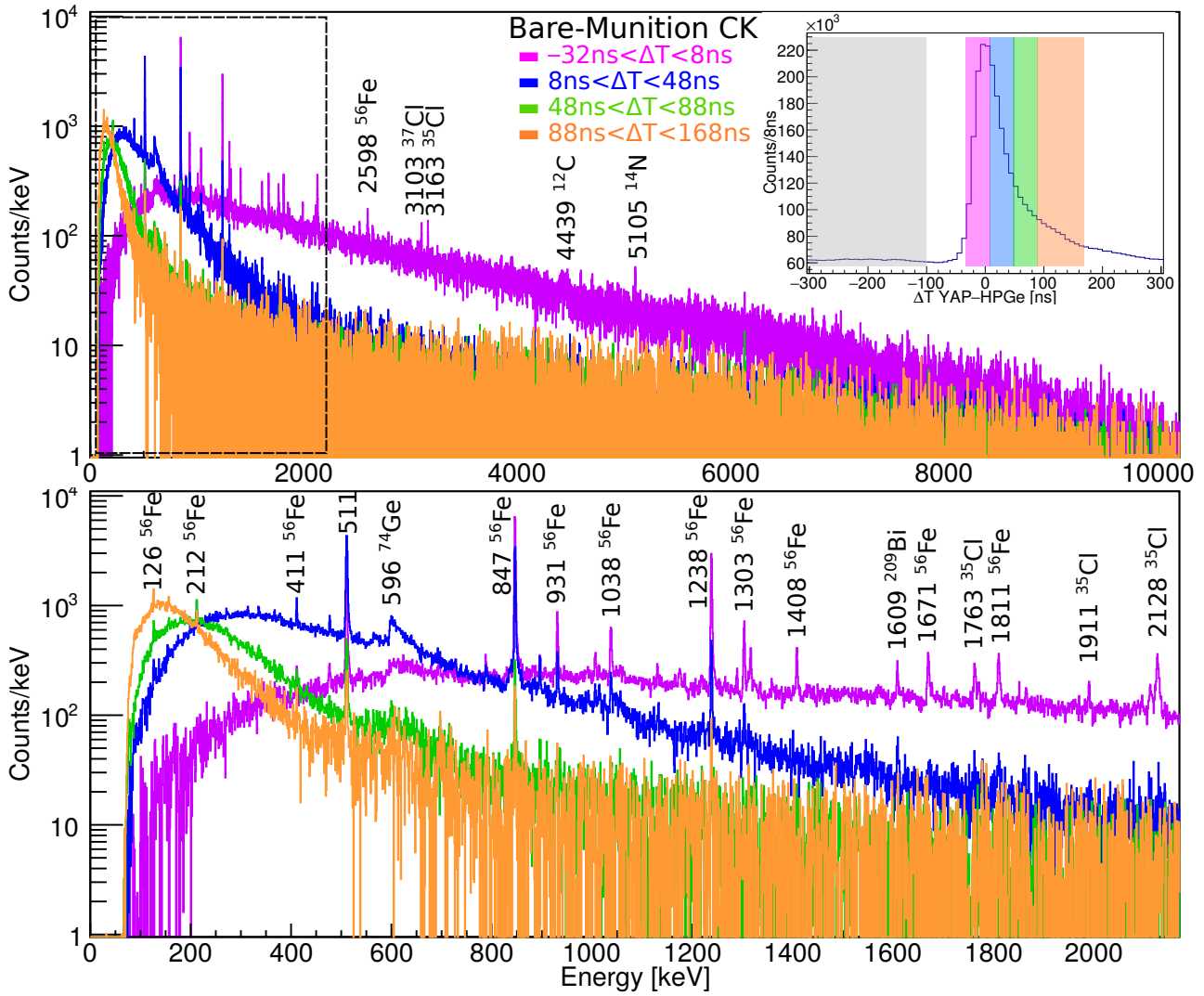


Figure 4: HPGe time-correlated AP-coincidence spectra recorded from the bare-munition CK simulant are shown in chronological increments from earliest (purple) to latest (orange). The inset shows the corresponding gate on the time spectrum for each HPGe coincidence spectrum. The random (uncorrelated) component of each is subtracted out using the gate between -100 ns and -300 ns (gray). The low-energy portions of the spectra have been expanded in the bottom half of the figure for ease of viewing the many γ -ray lines present there.

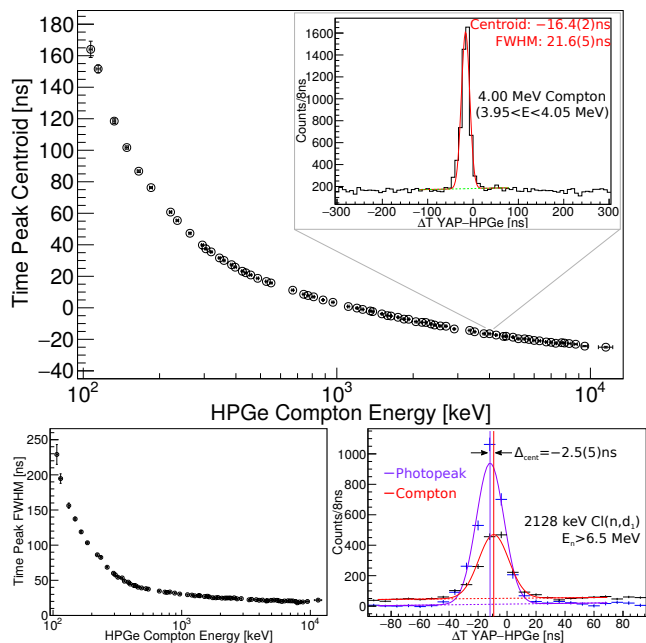


Figure 5: Centroids of correlated time peaks of the Compton continuum as a function of γ -ray energy are shown on top. Data were recorded from the bare-munition CK measurement. The time projection of a Compton slice centered at 4 MeV is shown in the inset with a Gaussian fit (red) to extract the centroid and FWHM. The bottom left shows the FWHM as a function of Compton energy. The bottom right shows the time projection of the Cl 2128-keV photopeak after subtraction of the underlying Compton compared to that of the latter along with their corresponding Gaussian fits.

suffering a 20% relative loss in precision of their quantified intensities. It was found that better results could be achieved simply by analyzing the low-energy 728-keV N peak using a separate AP-coincidence gate from the other higher-energy lines. The latter were analyzed using a 40-ns wide gate starting at -32 ns in the time spectrum while the former used a 48 ns wide gate starting at -16 ns. The high-energy time gate was optimized for γ rays with energies in the 2–3 MeV range, however good results were also achieved for the higher-energy γ -ray lines near 6 MeV, where shifting the time window to slightly earlier times did not significantly improve the precision of the latter.

Analysis of the 728-keV line, on the other hand, highly benefited from having its own, optimized coincidence gate due to the overall low emission intensity of that line, especially in the overpacked measurements where there was increased attenuation as well as higher background from greater neutron scatter and Compton events in the HPGe. Fig. 6 highlights the enhancement of this peak from the targeted AP-coincidence gate in both bare and overpacked CK measurements relative to the traditional, ungated spectra. Note that it is not even possible to observe the 728-keV line in the overpacked measurement without the aid of the AP coincidence requirement. These results are discussed along with the other γ -ray lines of interest in Section 4. It may be worth mentioning, however, the subset of other possible field-recoverable CW agents whose accu-

rate identification relies on even lower-energy characteristic γ rays. In particular, those containing arsenic (e.g. Lewisite), would almost definitely require their own separate targeted AP-gates to overcome the steep energy-walk response of HPGe in those spectral regions, assuming the standard leading edge timing discrimination continued to be employed. This would be alternative to using a single excessively wide coincidence gate that would result in a loss of sensitivity to low-intensity γ rays. The caveat is that, when assaying an item with unknown chemical fill, it may be necessary to acquire data in list mode, as was done in the present study, in order to retain sensitivity to both the high-energy and low-energy portions of the γ -ray spectrum within a single measurement. Otherwise multiple data acquisition channels incorporating a range of delays and gate widths may be needed to fully cover the entire γ -ray spectral region of interest for CW identification.

One other matter worth investigating was a potential reduction in unwanted γ -ray events from the MRC and vermiculite by utilizing a possible correlation between the n/α direction and the α signal pulse height. Although the R580 PMT that was coupled to the API-120 viewport to read out the α events from the internal YAP crystal did not have any position sensitivity, the YAP scintillator itself was fabricated with a grid pattern on its surface to help spatially discretize its light output as described by Bucher et al. (2022). With this consideration in mind and also the fact that the R580 diameter was significantly less than the YAP viewport diameter (1.5" compared to 1.9", respectively), various gates on the YAP pulse heights were examined to determine if any further reduction in γ -ray signal arising from regions outside the chemical simulant could be achieved. This was done for both overpacked CG and CK simulants. The intensity ratio of the 2128-keV Cl and 1434-keV Cr lines was analyzed for different cuts on the YAP pulse height spectrum. The 2128-keV Cl peak is the most intense, unique line arising from both simulants, while the 1434-keV Cr line is present in the stainless steel comprising the MRC, however not present in the steel comprising either of the mock munition shells. Therefore the Cl and Cr signals originate from maximally separated regions of the overpacked test items. The results are shown in Fig. 7. Clearly there is some spatial sensitivity achieved with this segmented YAP scintillator, however the separation between components is not enough to isolate the simulant signal from that due to the vermiculite. One limiting factor in this measurement was the suboptimal energy filter parameters used to process the YAP detector pulses, as discussed by Bucher et al. (2022) and mentioned in the timing discussion earlier, however the results do indicate substantial separation might be achieved in the future with improved filter settings and with the aid of a position-sensitive YAP detector readout.

The results presented in Section 4, thus, did not employ any YAP pulse height gates, but used only the optimized time gates mentioned earlier, with the 728-keV N line anal-

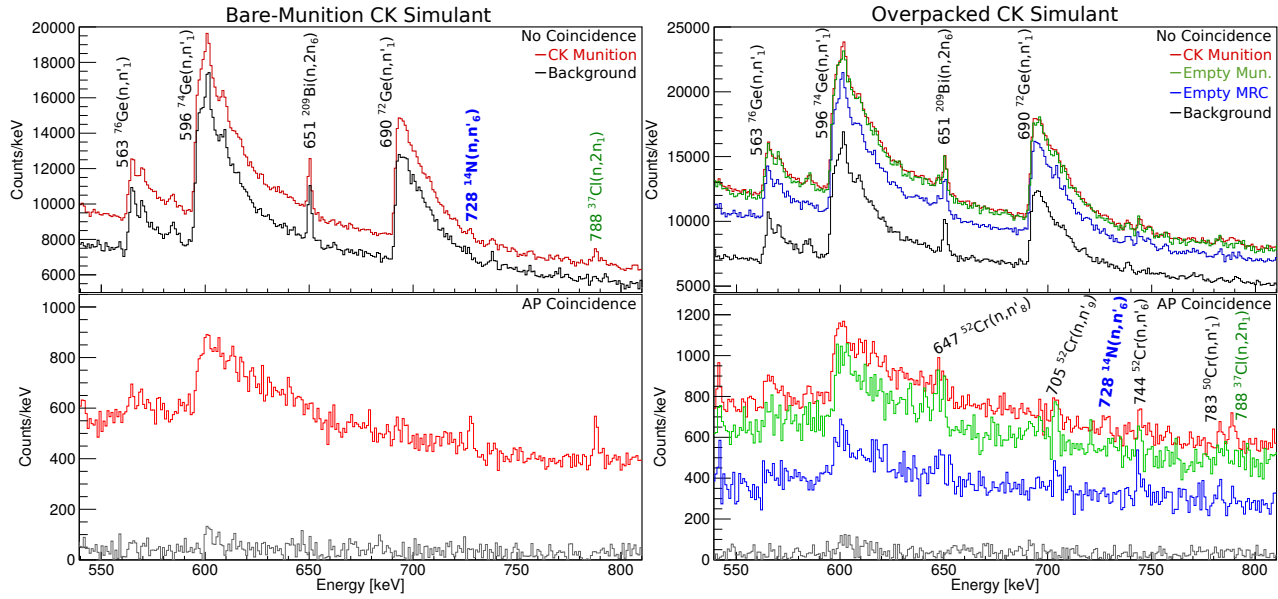


Figure 6: Bare-munition (left side) and overpacked (right side) CK simulant spectra shown in the energy region surrounding the N 728-keV peak. The traditional, ungated results are shown on top and optimized AP-gated results on the bottom. The simulant spectra are shown in red and background spectra in black/gray. The overpacked results include additional spectra recorded with an empty MRC (blue) and overpacked blank munition canister (green).

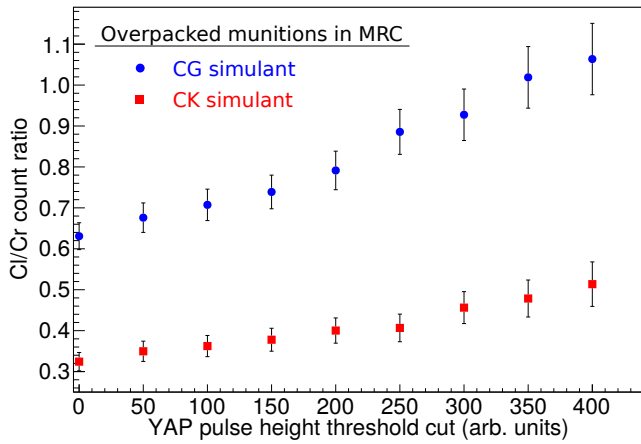


Figure 7: Observed Cl/Cr ratios in the AP-coincidence spectra for a range of YAP pulse height threshold cuts recorded from overpacked-munition CG (blue circles) and CK (red squares) simulant measurements. The outer steel MRC is the only material where Cr is present while the inner simulant is the only Cl-containing substance.

470
475
480
485
490
495

ysis utilizing a different gate from the other higher-energy lines of interest for the AP-coincidence spectra. The ungated HPGe spectra are also presented for comparison as they represent the traditional PGNAA approach. The relevant γ -ray peaks corresponding to the key elements Cl, C, N and O were analyzed in each spectrum and intensities extracted based on Gaussian fits or, in the case of the broad C peak, summation over the peak region with estimation of the Compton background provided by summation over a nearby region on the high energy side of the peak. The same procedure was carried out for the relevant peaks in the background spectra, namely those arising from C and O. The background intensities were then live-time normalized to the simulant results and subtracted where applicable. Regarding the various key elements, note that Cl exists only in the chemical simulants, while O is in the CG simulant, vermiculite, and concrete floor, N only detectable in the CK simulant, and C in both simulants, both steel munition containers, the MRC, and the polyethylene of the shadow shield. One unfortunate complication to the elemental analysis is the interference between the N 5105-keV line and the O DEP at 5107 keV. These cannot be resolved even with the superior energy resolution of a HPGe detector, however it is possible to detect an increased width of that peak indicating the presence of N. Therefore the FWHM and intensity ratios between the O DEP and 6129-keV full-energy peak (FEP) are also tabulated, in addition to the individual γ -ray peak intensities, to look for N in the presence of O. The Cl/C intensity ratio is also analyzed since it should be sensitive to the distinct chemical compositions of CK versus CG, the latter being a factor of 2 higher in the real CW agents.

4. Results & Discussion

The results presented in this section are meant to provide comparisons between the traditional PGNA and AP-coincidence technique in the discrimination of CK and CG-filled CW munitions in a realistic field scenario. As a baseline comparison, results from bare-munition (not overpacked in a MRC) measurements are presented first, with a small subset of qualitative results having already been reported by Bucher et al. (2022). Then the more field-relevant overpacked measurements are presented. For each comparison, a number of recorded spectra are shown: one set focused on the low-energy Cl regions between 1.6 and 3.2 MeV, and the other set focused on the higher-energy CNO region between 3.9 and 6.2 MeV. Side-by-side comparisons of the traditional (ungated) and AP-gated CK and CG simulant measurements are provided with their corresponding background spectra overlaid. Quantitative results extracted from the analysis of each spectrum are provided in tables focusing on the parameters identified in Section 3. Note that the relevant spectra pertaining to the N 728-keV γ -ray line analyses have already been presented in Section 3, however the quantitative results are included in the tables shown in this section. Each table compares analyses results from the CK and CG measurements for either the traditional or AP approach. Since the traditional approach relies heavily on background measurements and subsequent subtractions, two separate background measurements are considered for the overpacked items: the usual one performed in the field where nothing is near the generator/detector and one where an empty MRC is placed in the test position. As discussed shortly, the latter provides a better representation of the background present during the assessment of an overpacked munition. Moreover, the slight additional burden of adding an empty MRC to the standard background measurement may be well worth the improved accuracy of the field assessments, making it a practical consideration for future implementations. The AP technique, on the other hand, generally does not benefit from a background measurement/subtraction, so this is less of a consideration as that technique continues to be developed for possible field use.

4.1. Bare Munition Results

The relevant portions of the spectra obtained from the bare munition measurements are shown in Fig. 8. The ungated (i.e. no AP-coincidence), traditional PGNA spectra are shown in dark red with the background spectrum overlaid in black, while the corresponding AP-coincidence gated results are shown underneath each in red with their respective backgrounds overlaid in gray. The left side of Fig. 8 shows the lower-energy Cl region recorded for both the CK simulant (top set) and CG simulant (bottom set). In both cases, the AP technique does well to increase the relative intensities of the various Cl peaks, although the

strongest Cl peaks are still easily identified with the traditional method, in particular the 2128-keV line. In the ungated spectra, the 1763-keV Cl inelastic scatter line is also evident, although it sits on the shoulder of the much larger 1779-keV Si peak produced from the concrete floor. As pointed out by Bucher et al. (2022), this peak is even more intense in the background spectrum because the absence of the munition makes for a larger, unobstructed view of the floor by the detector. In the AP-gated spectrum, on the other hand, this background Si is removed, while the AP-background spectrum itself generally has very few peaks with only low intensities (Si being weakly present among them). The situation is a bit different in the CG spectra, because the employed simulant actually contains a small fraction of Si (Table 1). Therefore the Si line is also present in the AP-gated spectrum while the Cl lines are more intense in both gated and ungated CG spectra relative to those in the CK spectra due to the higher Cl mass fraction in the former. However the Si peak in the ungated background spectrum is still more intense than that in the ungated CG simulant spectrum despite its additional presence in the simulant itself. There are also a number of iron peaks present in the simulant and background spectra which primarily arise, respectively, from the mock munition containers and the steel cart supporting the HPGe detector.

Since both CK and CG produce strong Cl lines, in order to discriminate between the two, the measurements must also be sensitive to C, N, and O. The right side of Fig. 8 shows the higher-energy CNO region recorded for each simulant. As discussed by Bucher et al. (2022), the distinction between the two simulants is clear with the aid of the AP technique, where background O, like Si, arising mainly from the concrete floor, is completely removed. In the CK (CG) spectrum, this leaves only the C and N (O) lines from the chemical present, which means the other agent can be ruled out. As in the Cl region, the AP-gated background has little to no lines in the CNO region, so no subtraction is required. The traditional, ungated spectra, on the other hand, highlight the difficulty caused by the high background O and, to a lesser extent, C. In both simulant measurements, O is strongly present and with even greater intensity in the background measurement. Again this is due to the shielding of the detector's view of the ground by the munition itself. Comparing the two simulants, one observes a relatively stronger O intensity in the CG spectrum, due to the O mass fraction in that simulant, however the net intensity after background subtraction is still negative in either case (Table 3). Moreover, the strong background O DEP completely covers the weak N line at 5105 keV. It is, however, possible to observe its SEP at 4594 keV, along with the low-energy 728-keV N line (upper left of Fig. 6), albeit both with large statistical uncertainties. The only other elemental signature is the C intensity which can be used to determine the Cl/C ratio; the latter should differ by around a factor of two in the real agents. The quantitative results are provided in

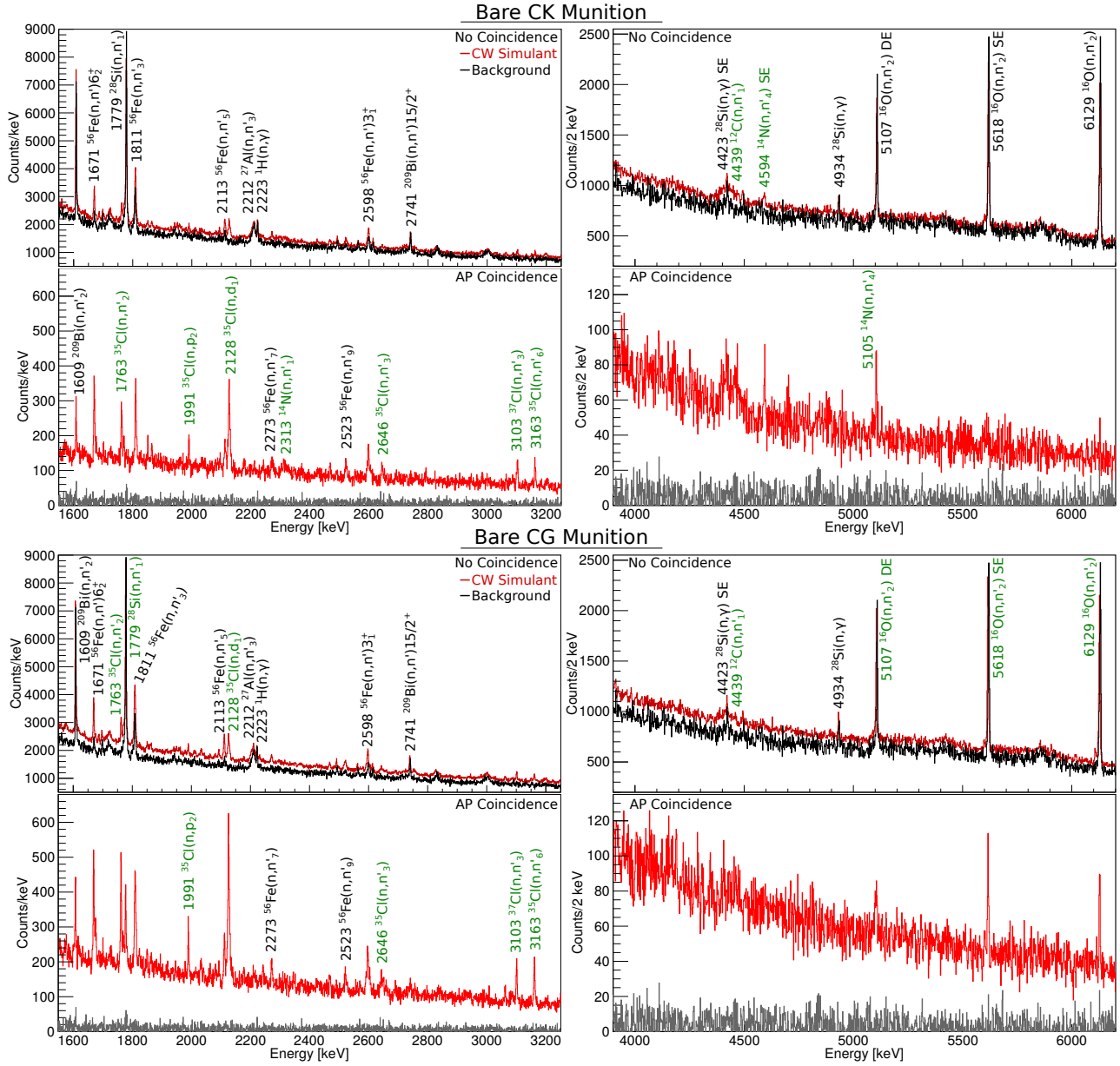


Figure 8: Bare-munition spectra recorded from the CK (top half) and CG (bottom half) simulants. The low-energy Cl-relevant region of the spectra are shown on the left side while the higher-energy CNO regions are displayed on the right. For each set, the traditional, ungated spectra are shown first (dark red) with the background (black) overlaid, while the corresponding AP-gated spectra (red) and their background (gray) are shown below.

Table 3 with comparison to those from the AP-gated spec-
tra. With the combination of detecting the two N peaks
and the measured Cl/C ratio, it may still be possible to
discriminate between the two CW agents with the tradi-
tional method, provided, of course, the bare munitions are
assayed. The difference in measured Cl/C ratios in terms
of 1σ units of uncertainty is 1.76 for the ungated results
which corresponds to a 92% confidence level, whereas with
the AP method this increases to 4.33σ , or >99.998% con-
fidence (Bevington and Robinson, 2003). Note that the
former is primarily limited by the C precision in CG after
background subtraction (Table 3), having a relatively low
mass fraction in that simulant. Nevertheless, considering
also the clear identification of N (O) in CK (CG) with
the AP technique, its discriminatory power is far superior
compared to the traditional method, the latter hinging on
fewer measurable parameters with higher uncertainties.

4.2. Overpacked Munition Results

As discussed earlier, in actual field measurements the
munitions are normally overpacked with vermiculite in a
sufficiently-sized MRC. This adds a number of extra chal-
lenges for the PGNAA assessment even if the AP tech-
nique is utilized. For one, the vermiculite contributes an
additional O signal, along with those from other light el-
ements like Mg, Al and Si (Papadopoulos et al., 2008),
which cannot be removed by the AP gate unless, perhaps,
a position-sensitive α detector is used, as mentioned in
Section 3. Additionally, the bulky steel MRC increases
the intensity of Fe lines in the spectra along with the al-
ready high Compton continuum. It also further attenuates
 γ rays of interest trying to escape the central chemical fill
of the munition and increases the flux of neutrons scattered
into the HPGe detector and its collimator. The overall ef-
fect is a loss of intensity of the chemical fill signature while
boosting the intensity of the background resulting in a sig-
nificant degradation of the precision. Furthermore, in the
case of the traditional PGNAA approach, the larger MRCs
block more of the HPGe detector's view of the ground thus
further reducing the sensitivity to elements such as O and
Si that are present in concrete and sandy soils resulting in
a large background oversubtraction of those.

The experimental results from the overpacked CK and
CG measurements are presented in Fig. 9 with correspond-
ing quantitative results provided in Table 4. The same rel-
evant spectral energy regions as shown in Section 4.1 are
again highlighted here, focusing on Cl lines in the lower-
energy portion and C, N, and O in the higher energy por-
tion (see the right side of Fig. 6 of Section 3 for the spectral
region surrounding the 728-keV N line). In addition to the
usual simulant (red) and background (black/gray) spectra,
results recorded from an empty MRC (blue) and empty
munition canister (identical to each of the ones used with
the CG and CK simulants, see Fig. 2) overpacked with ver-
miculite (green) are overlaid in Fig. 9. The background-
subtracted spectral analyses results, analogous to the ones
presented in Table 3 of Section 4.1, are given in Table 4

while the measured C and O fractional components in each
spectrum relative to the full simulant spectra are given in
Table 5. An in-depth discussion of the individual results
is provided in the following subsections, however a few
broad conclusions can be stated up front. First, as with
the bare munition measurements, the superiority of the
AP technique is clear when comparing the gated and un-
gated spectra. This is especially true in the lower-energy
simulant spectra where all the Cl lines are significantly
enhanced relative to the other lines present. Nevertheless,
the strongest Cl lines are also visible in the ungated spec-
tra allowing Cl to still be identified and quantified with
the traditional approach. In the higher-energy CNO re-
gion, on the other hand, and not to mention the 728-keV
region shown in Section 3, the advantages of the AP tech-
nique become much more critical for the discrimination
between the two agents as outlined below.

4.2.1. Ungated Discrimination

In both the CK and CG ungated spectra, the O in-
tensities are less than those observed in the background
spectrum resulting in negative O peak intensities in both
agents, as seen in the top left quadrant of Table 4, which
is similar to the situation observed for the bare munition
measurements in Section 4.1. The difference in this case,
however, is the large volume of vermiculite contributing an
O signal in both spectra. Although the bigger MRC does
block a proportionally wider area of the oxygen-containing
concrete floor, that void is filled with the oxygen-rich, al-
beit low-density, vermiculite positioned even closer to the
detector. The measured O fractions relative to the over-
packed simulant spectra are provided in Table 5. These
results can be compared between simulants along with the
net counts in Table 4. Each are indicative of the extra
O component in the CG simulant that is not present in
the CK one, however they are insufficient to provide any
conclusions about the presence of O in either case. The
situation can be somewhat improved by using the empty
MRC spectrum for background subtraction. The right side
of Table 4 can be used to compare the quantitative re-
sults obtained with this alternative background subtrac-
tion. Utilizing the empty MRC spectrum for the back-
ground subtraction, the net O counts in both simulants
become positive with the CG measurement yielding an O
FEP with an intensity greater than 4σ whereas the same
peak in the CK spectrum has an intensity of less than
 2σ . Obviously the overpacked blank munition spectra are
even more ideal background spectra, however such mea-
surements are not feasible in the field and, therefore, have
not been used for subtraction, although the quantitative
results corresponding to those spectra are included in Ta-
ble 5. The latter results indicate that the entire O signal
in the CK spectrum is due to the vermiculite, as expected,
while the CG spectrum does appear to have a slight excess
of O arising from the chemical simulant itself.

As with the O quantification, the C analysis may also
be improved using the empty MRC spectrum for back-

Table 3: Quantitative analysis results from the bare-munition CK and CG simulant measurements are compared. Results from the traditional, ungated approach are displayed on the left and those from the AP-approach are listed on the right. The ungated results have been background-subtracted for those peaks appearing in the background spectrum. The O double-escape (DE) to full-energy (FE) peak intensity (I) and width (W) ratios are calculated from the simulant spectra prior to background subtraction. Uncertainties for each parameter are listed in parentheses (1σ).

Bare Munition Results								
Parameter	Ungated Spectra (Bkgd Sub.)				AP-gated Spectra (No Bkgd. Sub.)			
	CK Sim.	CG Sim.	Diff.	Diff./ σ	CK Sim.	CG Sim.	Diff.	Diff./ σ
Cl	4430(400)	6250(410)			1643(73)	3121(92)		
C	3180(590)	1800(580)			1058(82)	582(93)		
N 728	950(230)	N/A		4.04	319(60)	N/A		5.29
N SE	610(160)	N/A		3.78	130(33)	N/A		3.96
O DE (N FE)	51(190)	-140(260)			120(21)	148(44)		
O SE	-830(220)	-300(220)			N/A	191(30)		
O FE	-1170(290)	-750(210)			N/A	168(25)		
O $I(\frac{DE}{FE})$	0.676(32)	0.599(37)	0.077(49)	1.58	N/A	0.88(29)		
O $W(\frac{DE}{FE})$	0.872(33)	0.794(30)	0.078(45)	1.74	N/A	2.46(76)		
Cl/C	1.39(29)	3.5(11)	2.1(12)	1.76	1.55(14)	5.36(87)	3.81(88)	4.33

Table 4: Quantitative analysis results from the overpacked-munition CK and CG simulant measurements are compared. Results from the traditional, ungated approach are displayed on the top half and those from the AP-approach are listed on the bottom. Two separate background subtractions were examined: results using the conventional one where nothing is near the detector/generator are listed on the left while the right side shows results using the empty MRC spectrum as the background (see text). Peaks that are not present in the background spectra do not require any subtraction. For the AP-gated results, the only peak affected by the different background measurements is that arising from C. The O double-escape (DE) to full-energy (FE) peak intensity (I) and width (W) ratios are calculated from the simulant spectra prior to background subtraction and are, hence, unaffected by whichever spectrum is used for background. Uncertainties for each parameter are listed in parentheses (1σ).

Overpacked Munition Results								
Parameter	CK Sim.	CG Sim.	Diff.	Diff./ σ	CK Sim.	CG Sim.	Diff.	Diff./ σ
		Ungated–Normal Bkgd Sub.				Ungated Blank MRC Sub.		
Cl	3160(390)	4440(450)				Same		
C	2870(570)	2650(570)			2570(640)	2350(640)		
N 728	Too weak	N/A				Same		
N SE	420(110)	N/A		3.93		Same		
O DE (N FE)	-14(270)	92(270)			200(280)	300(280)		
O SE	-780(300)	-290(220)			120(300)	590(220)		
O FE	-510(290)	-74(210)			530(300)	940(220)		
O $I(\frac{DE}{FE})$	0.635(45)	0.608(38)	0.026(58)	0.45		Same		
O $W(\frac{DE}{FE})$	0.869(35)	0.830(34)	0.039(49)	0.80		Same		
Cl/C	1.10(26)	1.67(40)	0.57(47)	1.21	1.23(34)	1.89(54)	0.66(64)	1.02
	AP-gated–No Bkgd Sub.				AP-gated Blank MRC Sub.			
Cl	1159(70)	1839(80)				Same		
C	1120(100)	800(100)			840(150)	530(150)		
N 728	335(93)	N/A		3.60		Same		
N SE	150(38)	N/A		3.95		Same		
O DE (N FE)	261(42)	186(30)				Same		
O SE	150(29)	353(34)				Same		
O FE	190(28)	319(34)				Same		
O $I(\frac{DE}{FE})$	1.37(30)	0.58(11)	0.79(32)	2.45		Same		
O $W(\frac{DE}{FE})$	1.72(39)	0.84(19)	0.88(43)	2.05		Same		
Cl/C	1.04(11)	2.30(31)	1.26(33)	3.79	1.38(26)	3.46(99)	2.1(10)	2.04

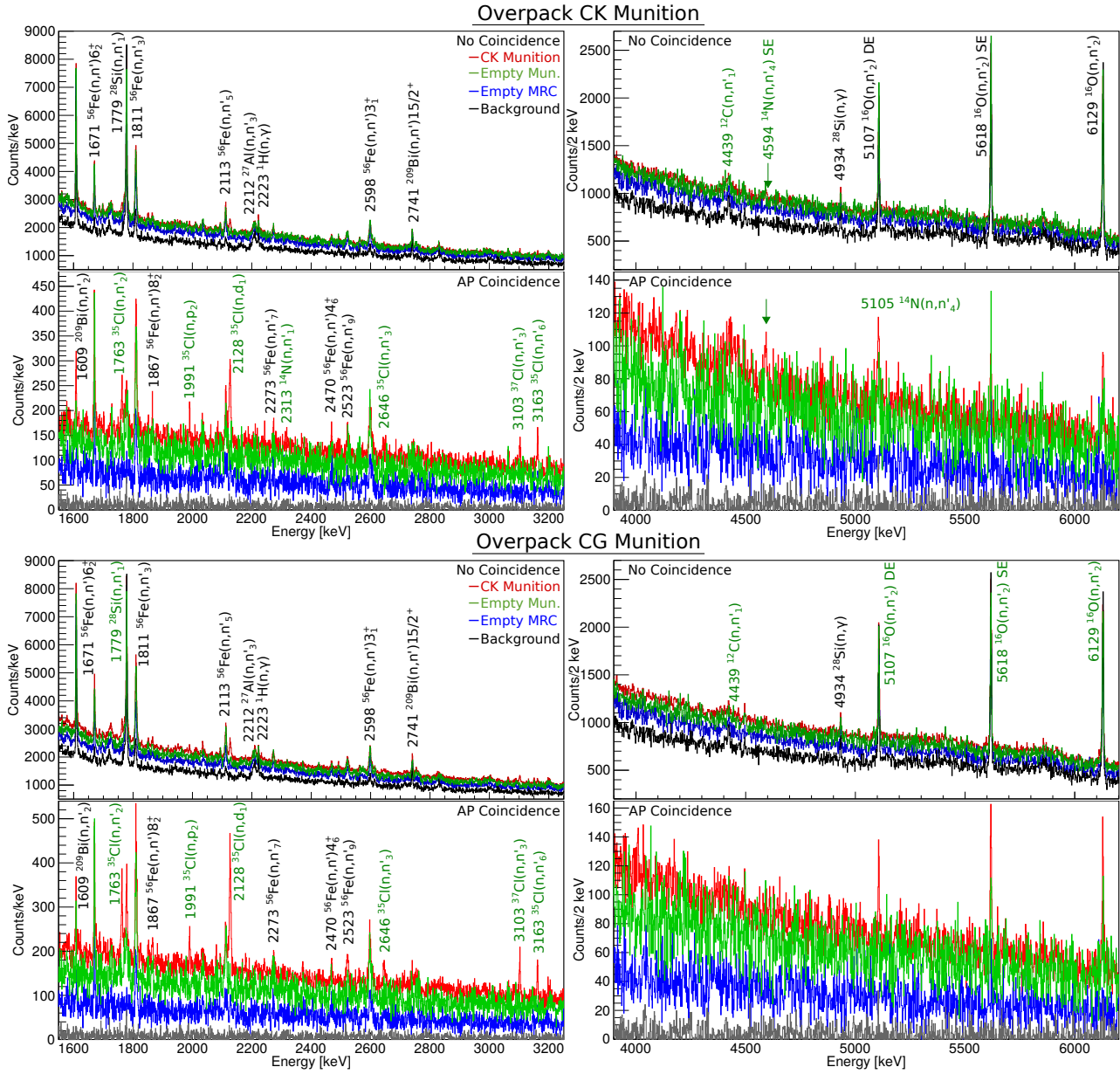


Figure 9: Overpacked-munition spectra recorded from the CK (top half) and CG (bottom half) simulants. The low-energy Cl-relevant region of the spectra are shown on the left side while the higher-energy CNO regions are displayed on the right. For each set, the traditional, ungated spectra are shown first (dark red) with the background (black) overlaid, while the corresponding AP-gated spectra (red) and their background (gray) are shown below. Also included for each set of spectra are ones recorded from an empty MRC (blue) and an empty mock munition case, identical to the one used with each simulant, overpacked with vermiculite in the MRC (green).

Table 5: Carbon and oxygen peak intensity ratios of each spectrum relative to the overpacked CK (left) and CG (right) simulant spectra are listed with uncertainties given in parentheses (1σ). Results for the ungated spectra are shown in the top half while the AP-gated results are shown on the bottom.

Peak	Bkgd/CK	MRC/CK	Blank/CK	Bkgd/CG	MRC/CG	Blank/CG
Ungated						
O DEP	1.00(7)	0.95(7)	1.00(8)	0.98(7)	0.92(7)	0.85(7)
O SEP	1.14(6)	0.98(5)	1.08(6)	1.05(4)	0.90(4)	0.97(4)
O FEP	1.09(5)	0.91(5)	1.03(5)	1.01(3)	0.85(3)	0.91(3)
C	0.64(6)	0.68(7)	0.85(7)	0.66(7)	0.70(8)	0.90(7)
AP-gated						
O DEP	N/A	N/A	0.43(15)*	N/A	N/A	0.37(11)*
O SEP	N/A	N/A	1.01(32)	N/A	N/A	0.67(15)
O FEP	N/A	N/A	0.99(35)	N/A	N/A	0.36(11)
C	N/A	0.25(10)	0.29(14)	N/A	0.34(14)	0.47(19)

* O DEP not observed in blank munition spectra; intensity estimated from FEP (see text)

ground subtraction. Table 5 shows perhaps a small C contribution from the stainless steel body of the MRC, however a larger contribution comes from the munition body. The latter probably contains a similar fraction of C, but also has the bulk of its material positioned closer to the detector, on average, and certainly results in increased neutron reflection into the carbon-rich polyethylene shield block between the detector and generator. In either case, this C contribution cannot be subtracted out of the field measurements, however, using the empty MRC spectrum for background subtraction, a lower net C intensity is obtained in Table 4. This in turn leads to a greater absolute separation in Cl/C ratios between the CK and CG measurements, yet the larger separation is offset by an overall increase in uncertainty, due to the larger relative uncertainty in C intensity obtained using the MRC subtraction (the Cl analysis is unaffected since it is not present in either background spectrum). This effectively degrades the discriminability potential of the Cl/C ratio since the relative separation is reduced to 1.0σ compared to the original 1.2σ . Regardless of which background subtraction is used, however, the separation is not enough to discriminate between the two agents.

Then the only remaining parameters that can be used to discriminate the two agents must come from the N analysis. As with the bare munition measurements, the N FEP at 5105 keV is covered by the O DEP. With this interference, the only possible indications of N presence would show up as increased O DEP/FEP intensity and width ratios. Unfortunately, considering the experimental uncertainties of each parameter listed in Table 4, it is not possible to identify the N component in the O DEP of the CK spectrum. Moreover, the 728-keV N line, which was visible in the ungated bare munition spectrum, is too weak to observe in the overpacked configuration due to the increased attenuation and higher background arising in the latter. That leaves only the N SEP at 4594 keV which is observed in the CK spectrum with an intensity/uncertainty ratio of 3.9σ , similar to the bare munition results and apparently less affected by attenuation and higher background

than the 728-keV line because of its much higher energy. Although a positive N detection is enough to rule out a possible CG agent fill, having to rely solely on the observation of the weak N SEP is not ideal and precludes any confident discrimination between the two.

4.2.2. AP-gated Discrimination

Once the AP-coincidence requirement is imposed, the situation is much improved, although the O signal from the vermiculite still presents a challenge. In the lower right AP-gated spectrum of Fig. 9, the O from the CG simulant is clearly higher than that due to the vermiculite (green), while no O is present in either the empty MRC (blue) or regular background (gray) spectrum. In the CK simulant measurement (upper right), on the other hand, the measured O is consistent with that found from the vermiculite with the blank munition. Table 5 (lower left) confirms that the measured O FEP and SEP intensities are consistent between the CK simulant and blank munition spectra. In the case of CG, the O intensity is roughly equally composed of vermiculite and the simulant. In both blank munition spectra, the O DEP was not observed due to its lower intensity relative to the FEP and SEP and also the low statistics from the shorter run times. Therefore the O DEP intensity is estimated as $I_{\text{DEP}} = 0.6 * I_{\text{FEP}}$ which is based on observations in the various ungated spectra as well as the AP-gated CG simulant spectrum (see Tables 3 & 4). This produces a O DEP blank/simulant ratio in the CG measurement that is consistent with the O FEP and SEP ones. The CK simulant, on the other hand, has an excess of counts in the DEP relative to the FEP and SEP which is certainly due to the N FEP at 5105 keV. Indeed, the corresponding N SEP at 4594 keV is also observed.

As with the bare munition measurements, no background subtraction is needed for the AP-gated results. The raw spectral counts are shown in Table 4. The O FEP and SEP counts in the CK measurement are due to the vermiculite while the excess in the DEP is from N. This is reflected in the DEP/FEP intensity ratio when compared

to that observed in the CG measurement. A difference of more than 2.4σ is observed between the two agents. Moreover, unlike in the ungated results, an excess width is also observed in the O DEP in the CK measurement. Comparing the DEP/FEP width ratios in the two spectra results in another difference greater than 2σ . These combined with the observation of the N SEP as well as the N 728-keV peak (Fig. 6), the latter not visible without the aid of the AP-coincidence gate, provide added confidence to the discrimination of CK from CG.

Further discrimination is provided from the C analysis and determination of the Cl/C ratios. The bottom line of Table 4 shows this parameter which provides the greatest separation between the two agents with 3.8σ difference, similar to that observed in the bare munition results. Realizing, as mentioned earlier, that the MRC does contribute a small fraction of the C intensity, the C signal was also analyzed by subtracting the component found in the (AP-gated) empty MRC spectrum. This significantly reduced the net C counts, especially in the CG measurement where C is a smaller mass fraction of that simulant, which in turn further widened the absolute Cl/C ratios between the two simulants. Despite this improvement, however, the additional uncertainty created from the C background subtraction actually made the relative difference much less having only 2σ deviation. Thus the loss in statistical precision caused by the relatively small background subtraction made the situation worse. Therefore it is better to forgo any background subtraction in the AP results with the minor trade-off of keeping the systematic effect caused by the MRC. In practice, this is not very consequential since a similar effect is caused by the munition casing itself which is impossible to account for in actual field measurements.

One other potential systematic effect on the C analysis to consider might be the O contribution to the 4439-keV peak through the $^{16}\text{O}(n,n'\alpha_1)$ reaction. However, recent pure-element spectra measured with a similar AP-based PGNAA device (Sudac et al., 2020) as well as results reported with a larger scale AP-neutron interrogation system (Pino et al., 2021) both indicate this contribution is small compared to the 6129-keV $^{16}\text{O}(n,n'_2)$ reaction. Given the relative counts observed between the two lines in the present measurement, the sizable statistical uncertainties, and the systematic errors already discussed, this effect appears to be rather insignificant. Despite these few systematic uncertainties, the overall combination of measured Cl/C ratio, O DEP/FEP intensity and width ratios, and observation of the N 4594-keV and 728-keV lines obtained with the AP technique enables a much more confident discrimination between overpacked CG- and CK-filled munitions when compared to the results obtained with the traditional, ungated PGNAA approach.

5. Conclusions

This work assessed the discriminatory power of the background-suppressing associated particle technique for

identifying simulants of CG and CK chemical warfare agents contained within mock 4.2-inch (11 cm) mortar shells overpacked with vermiculite in MRCs. Quantitative results are compared with those obtained for bare munition measurements, first reported in by Bucher et al. (2022), along with ones obtained with the traditional, PGNAA approach for both configurations. The successful discrimination of the two agents using the traditional PGNAA approach relies primarily on the confident detection of the weak N SEP at 4594 keV from CK, which is strongly dependent on the amount of agent present in the munition, the degree of attenuation from the munition body and employed MRC, and the height of the Compton continuum produced by the surrounding materials. The situation may be slightly improved by using an identical empty MRC in the background measurement to improve the sensitivity to O that would be weakly present in a CG chemical fill.

The AP-technique, on the other hand, had much better sensitivities to O in the CG simulant as well as N in the CK simulant, the latter based on its effect on the observed O DEP/FEP intensity and width ratios when present along with a heightened sensitivity to the low-energy 728-keV line. Moreover, the discriminability also benefited from increased precision on the Cl/C ratios which was mainly due to improved C sensitivity and the nonnecessity to perform a background subtraction for the spectral analyses. Generally speaking, relative uncertainties were improved by about a factor of two using the AP-technique. This better precision allowed for a fivefold increase in the number of statistically-significant ($>2\sigma$) discriminating spectral observables between the two simulants as compared to the traditional approach which yielded only one. Thus the discriminatory power of the AP-technique remained robust for the overpacked measurements.

In these measurements, great care was taken to optimize the timing parameters of the AP coincidence gate to limit the number of random background coincidences requiring subtraction, including the use of a separate targeted gate for the N 728-keV γ -ray analysis. The latter became necessary to overcome a substantial signal pulse time walk observed in the HPGe detector with decreasing γ -ray energy. Although this was easily accomplished through offline sorting of the recorded list mode data, the situation may become more complicated for performing online field analyses, particularly in dealing with CW agents that emit very low-energy γ rays where the HPGe time response is extremely sensitive, such as those containing arsenic. Additional improvements can likely be made using constant fraction timing which should largely eliminate the amplitude walk effect and also narrow the timing resolution relative to that achieved in the present study using leading edge timing. This would, in turn, allow for narrower coincidence gates which would reduce the number of random coincidence events that need to be subtracted, thus improving the overall precisions that could be achieved, particularly for the low-intensity peaks like those from nitrogen. Even with suboptimal timing properties, however,

the good energy resolution achieved with this detector is considered a favorable trade-off for these types of field measurements, as discussed by Bucher et al. (2022). On the other hand, the method might be further improved in the future through the use of a position-sensitive PMT with the AP α -detector, which may help to suppress some of the background from the MRC and vermiculite, as was indicated in the present work by examining α pulse height gates.

6. Acknowledgments

The authors would like to acknowledge A.J. Caffrey (INL) and W. Hennig (XIA) for helpful discussions and also E. Lumley (INL) for help fabricating mechanical components. This work was supported by the U.S. Army Chemical Materials Activity (CMA) Recovered Chemical Materiel Directorate (RCMD) and through the INL Laboratory Directed Research & Development (LDRD) Program under DOE Idaho Operations Office Contract DE-AC07-05ID14517.

References

- Bevington, P.R., Robinson, D.K., 2003. Data Reduction and Error Analysis for the Physical Sciences. McGraw-Hill, New York, NY.
- Brun, R., Rademakers, F., 1997. Root – An object oriented data analysis framework. Nucl. Instrum. Methods Phys. Res. A 389, 81–86. doi:[https://doi.org/10.1016/S0168-9002\(97\)00048-X](https://doi.org/10.1016/S0168-9002(97)00048-X). see also <https://root.cern/>.
- Bucher, B., Seabury, E.H., Hix, J., Krebs, K.M., Wharton, C.J., McConchie, S.M., Hausladen, P.A., 2022. Assessment of the associated particle technique with high-resolution gamma-ray spectroscopy for in-field identification of chemical warfare agents and explosives. Nucl. Instrum. Methods Phys. Res. A 1032, 166651. doi:10.1016/j.nima.2022.166651.
- Caffrey, A.J., Cole, J.D., Gehrke, R.J., Greenwood, R.C., 1992. Chemical Warfare Agent and High Explosive Identification by Spectroscopy of Neutron-Induced Gamma Rays. IEEE Trans. Nucl. Sci. 39, 1422–1426. doi:10.1109/23.173218.
- Campbell, J., 2022. Army continues work to dispose of chemical weapons. https://www.army.mil/article/253326/army_continues_work_to_dispose_of_chemical_weapons. U.S. Army press release.
- Carlson, J.S., Crocker, R.W., 2021. Phosgene Neutralization Chemistry for the Explosive Destruction System (EDS). SAND2021-11385. Sandia National Laboratory. doi:<https://doi.org/10.2172/1820308>.
- Carton, G., Hoffman, D., King, J.C., 2016. Recovering chemical warfare materiel. Military Eng. 108, 60–62. URL: <http://www.jstor.org/stable/26357624>.
- Chichester, D.L., Lemchak, M., Simpson, J.D., 2005. The API 120: A portable neutron generator for the associated particle technique. Nucl. Instrum. Methods Phys. Res. B 241, 753–758. doi:10.1016/j.nimb.2005.07.128.
- Chichester, D.L., Seabury, E.H., Zabriskie, J.M., Wharton, J., Caffrey, A.J., 2009. Dose profile modeling of Idaho National Laboratory's active neutron interrogation laboratory. Appl. Radiat. Isot. 67, 1013–1022. doi:10.1016/j.apradiso.2009.01.002.
- Compton, J.A.F., 1987. Military Chemical and Biological Agents. The Telford Press, Caldwell, NJ.
- DENIX - DoD Environment, Safety and Occupational Health Network and Information Exchange, . History of United States' involvement in chemical warfare. <https://www.denix.osd.mil/rcwmpprogram/history/index.html>. Accessed June 2022.
- Fazili, Y., Bistarkey, D., Ducasse, A., 2022. U.S. meets milestone in chemical weapons stockpile destruction. <https://www.defense.gov/News/News-Stories/Article/Article/3036463/us-meets-milestone-in-chemical-weapons-stockpile-destruction/>. U.S. Department of Defense press release.
- Idaho National Laboratory, . INL National & Homeland Security Fact Sheet: Portable Isotopic Neutron Spectroscopy. <https://factsheets.inl.gov/FactSheets/Portable%20Isotopic%20Neutron%20Spectroscopy%20System.pdf>. Accessed September 2022.
- Knoll, G.F., 1979. Radiation Detection and Measurement. John Wiley & Sons, New York.
- National Center for Biotechnology Information, . PubChem Compound LCSS for CID 7954, Cyanuric chloride. <https://pubchem.ncbi.nlm.nih.gov/compound/Cyanuric-chloride#datasheet=LCSS>. Accessed June 2022.
- National Research Council, 2012. Remediation of Buried Chemical Warfare Materiel. The National Academies Press, Washington, DC. doi:10.17226/13419.
- Organisation for the Prohibition of Chemical Weapons, . Chemical Weapons Convention. <https://www.opcw.org/chemical-weapons-convention>. Accessed June 2022.
- Papadopoulos, A.P., Bar-Tal, A., Silber, A., Saha, U.K., Raviv, M., 2008. 12 - Inorganic and synthetic organic components of soilless culture and potting mixes, in: Soilless Culture. Elsevier, pp. 505–543. doi:<https://doi.org/10.1016/B978-044452975-6.50014-9>.
- Pino, F., Fontana, C.L., Nebbia, G., Pedersen, B., Varasano, G., Sardet, A., Carasco, C., Pérot, B., Seibert, A.G., Poli, J.P., Sannié, G., Iovene, A., Tintori, C., Sibczynski, P., Grodzicki, K., Swiderski, L., Moretto, S., 2021. Detection module of the C-BORD Rapidly Relocatable Tagged Neutron Inspection System (RRTNIS). Nucl. Instrum. Methods Phys. Res. A 986, 164743. doi:10.1016/j.nima.2020.164743.
- Sudac, D., Pavlovic, M., Obhodas, J., Nad, K., Orlic, Z., Uroic, M., Korolija, M., Rendic, D., Meric, I., Pettersen, H.E.S., Valkovic, V., 2020. Detection of Chemical Warfare (CW) agents and the other hazardous substances by using fast 14 MeV neutrons. Nucl. Instrum. Methods Phys. Res. A 971, 164066. doi:10.1016/j.nima.2020.164066.
- U.S. Army Chemical Materials Activity, a. Recovered Chemical Materiel Directorate Fact Sheet: Explosive Destruction System (EDS) Overview. https://www.cma.army.mil/wp-content/uploads/2021_04_30_RCMD_FS_EDS-OVERVIEW_single_LR.pdf. Accessed June 2022.
- U.S. Army Chemical Materials Activity, b. Recovered Chemical Materiel Directorate Fact Sheet: Multiple Round Container (MRC). https://www.cma.army.mil/wp-content/uploads/2021_03_04_RCMD_FS_MRC_LR.pdf. Accessed June 2022.
- U.S. Army Chemical Materials Activity, c. Recovered Chemical Materiel Directorate Fact Sheet: Portable Isotopic Neutron Spectroscopy (PINS). https://www.cma.army.mil/wp-content/uploads/2021_03_08_RCMD_FS_PINS_LR.pdf. Accessed June 2022.
- XIA, . Pixie-4 Express User Manual. <https://s3.us-west-1.amazonaws.com/download.xia.com/products/pixie4/documents/manuals/XIA-Pixie-4e-MAN-Users-Manual-2019-06-17.pdf>. Accessed September 2022.